

Hyperspectral Tree Species Classification of Japanese Complex Mixed Forest With the Aid of Lidar Data

Tomohiro Matsuki, Naoto Yokoya, *Member, IEEE*, and Akira Iwasaki

Abstract—The classification of tree species in forests is an important task for forest maintenance and management. With the increase in the spatial resolution of remote sensing imagery, individual tree classification is the next target of research area for the forest inventory. In this work, we propose a methodology involving the combination of hyperspectral and LiDAR data for individual tree classification, which can be extended to areas of shadow caused by the illumination of tree crowns with sunlight. To remove the influence of shadows in hyperspectral data, an unmixing-based correction is applied as preprocessing. Spectral features of trees are obtained by principal component analysis of the hyperspectral data. The sizes and shapes of individual trees are derived from the LiDAR data after individual tree-crown delineation. Both spectral and tree-crown features are combined and input into a support vector machine classifier pixel by pixel. This procedure is applied to data taken over Tama Forest Science Garden in Tokyo, Japan, to classify it into 16 classes of tree species. It is found that both shadow correction and tree-crown information improve the classification performance, which is further improved by postprocessing based on tree-crown information derived from the LiDAR data. Regarding the classification results in the case of 10% training data, when using the random sampling of pixels to select training samples, a classification accuracy of 82% was obtained, while the use of reference polygons as a more practical means of sample selection reduced the accuracy to 71%. These values are, respectively, 21.5% and 9% higher than those that are obtained using hyperspectral data only.

Index Terms—Classification, data fusion, forest, hyperspectral data, LiDAR.

I. INTRODUCTION

THE sustainable management of forests is an important task from the viewpoint of the environment and economy. Forest inventory, which is the systematic collection of data and information, such as the tree species, heights, diameters at breast height, site qualities, ages and, so forth, is used to help sustainable forest ecosystems. Therefore, tree species classification is an important issue in the study of forest management and land cover [1]. Periodic field surveys by experts require a large amount of time and human resources. Since

Manuscript received September 30, 2014; revised February 03, 2015; accepted March 13, 2015. The hyperspectral data and LiDAR data were provided by Japan Space Systems (JSS). This work was supported under the contract with the National Institute of Advanced Industrial Science and Technology (AIST) as part of the Hyperspectral Imager Suite (HISUI) project.

T. Matsuki is with the Department of Aeronautics and Astronautics, University of Tokyo, Tokyo 113-8656, Japan (e-mail: matsuki@sal.rcast.u-tokyo.ac.jp).

N. Yokoya and A. Iwasaki are with the Research Center for Advanced Science and Technology, University of Tokyo 153-8904, Tokyo, Japan.

Color versions of one or more of the figures in this paper are available online at <http://ieeexplore.ieee.org>.

Digital Object Identifier 10.1109/JSTARS.2015.2417859

remote sensing enables wide-area observation at a single time, its contribution to tree species classification over forests is expected [2], [3]. By monitoring forests frequently, remote sensing is expected to abstract information that will help forest management to preserve biodiversity, which is an important index used to evaluate environmental health. Remote sensing is also important for estimating biomass and the natural carbon sink to study regional environments.

In recent years, many researchers have worked on the classification or identification of tree species using remote sensing techniques. Since airborne hyperspectral sensors have several tens of observation bands and high spatial/spectral resolution, a continuous spectrum can be obtained that enables more detailed analysis of the specified spectral profiles of individual trees at a pixel level [4]–[6]. Spectral–spatial approaches, such as the use of morphological profiles, are effective for the accurate classification of hyperspectral data using both spectral and spatial features, which are often concatenated into feature vectors and classified by a support vector machine (SVM) [7]. In a forest, the pixel values corresponding to a tree crown are influenced by the illumination of sunlight and the tree-crown shape, which make it difficult to extract spatial features of tree crowns only based on hyperspectral imagery without suitable preprocessing to take account of variations in the illumination.

Light detection and ranging (LiDAR) is a powerful tool for obtaining canopy height models (CHMs) by using return pulses from above the tree crown and terrain surface [8]. Since LiDAR is an active remote sensing instrument, it is unaffected by the illumination conditions of sunlight. Using CHMs, individual tree heights, crown areas, and shapes are obtained, which are used in the segmentation of forests into tree crowns [9]. Such information is used to identify species of individual trees only using LiDAR data [10]. Full-waveform LiDAR records the complete waveform of a backscattered signal echo, which is used to reconstruct tree structures, such as the stem volume and diameter at breast height [11]. Therefore, tree-crown features, such as the tree size and shape, obtained from LiDAR-derived CHMs are also expected to be useful in tree species classification.

In recent years, the fusion of hyperspectral and LiDAR data for classification has been studied [12]–[19]. Many researchers use LiDAR data for preprocessing to find trees by thresholding CHMs. The illumination condition is also obtained from CHMs, and thus the masks of shadow areas are created [14]. Raw height data and pixel-level statistics are used as features of tree crowns, which improve the classification accuracy [15], [16]. Individual tree-crown delineation is effective for

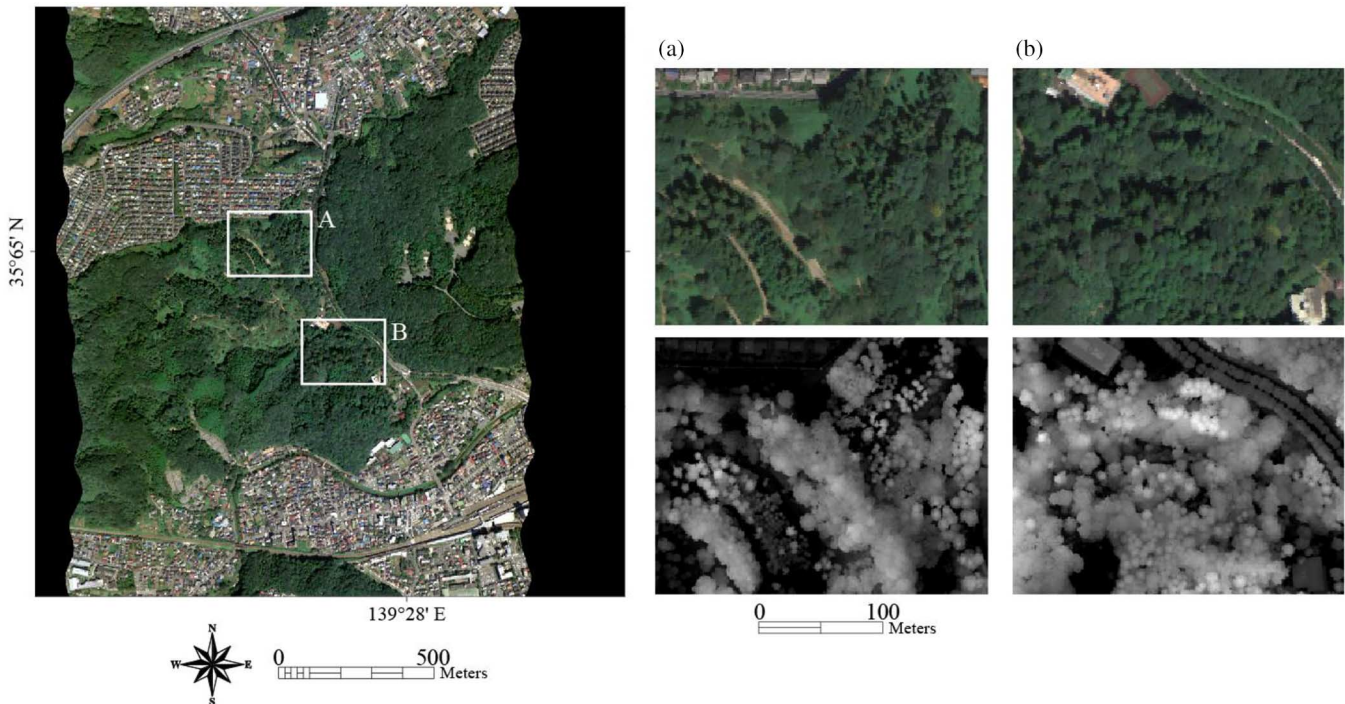


Fig. 1. (Left) Whole RGB image obtained using hyperspectral data. (Right) Enlarged RGB images of study areas A and B with CHM derived from LiDAR data.

preprocessing and postprocessing in the classification procedure [17]. By treating pixels in a tree crown together, similar merits to those of spectral–spatial techniques are expected. Volumetric canopy profiles [18] and structural metrics obtained from point clouds by waveform LiDAR [19] further improve the capture of tree-crown information.

In this work, we propose a methodology to classify tree species by coupling hyperspectral and LiDAR data. After shadow correction is applied to hyperspectral data to decrease the common source of intensity variability, spectral features are obtained by extracting principal components. Tree-crown features, such as tree heights, sizes, and shapes, are derived by tree-crown delineation and shape fitting to CHMs. Spectral and tree-crown features are fused and then input to the SVM classifier. A crown-preserving smoothing filter based on tree-crown information is applied as a postprocessing technique to improve the classification. We apply the procedure to the challenging tree species classification problem of Japanese complex mixed forests and show its effectiveness.

II. MATERIALS

A. Study Area

Japan is located in East Asia and consists of subarctic, temperate, and subtropical climate zones. Therefore, Japanese forests contain a wide range of tree species. The study area is Tama Forest Science Garden in the western region of Tokyo [20], which is managed by the Forestry and Forest Products Research Institute, Japan. This forest has an area of 56 ha and includes a special region containing many tree species found in gardens. Since broadleaf evergreen trees from the warm temperate zone, deciduous trees from the cool temperate

zone, and conifers from the subarctic zone coexist in the garden, it is suitable for investigating tree species classification in Japan.

B. Remote Sensing Data

The left image in Fig. 1 is a color image obtained using hyperspectral data from the 654, 552, and 449 nm bands, corresponding to red, green, and blue (RGB), respectively. The right images in Fig. 1 show enlarged RGB images of study areas A and B and the respective CHM images derived from LiDAR data. The data were obtained by airborne sensors on September 10, 2009, and provided by Japan Space Systems. Since the data were obtained in early fall, all the trees had green leaves, making it difficult to use their colors for analysis. The hyperspectral data were obtained by CASI-3 with 72 bands covering wavelengths of 400–1050 nm. The ground sampling distance of the hyperspectral data was 1 m, and the data were resampled to obtain an orthorectified data cube using a digital surface model (DSM) derived from LiDAR data. To avoid the effects of the bidirectional reflectance distribution function, the data in the target areas were obtained along the nadir path. The acquired data were processed to obtain radiance data using the instrumental characteristics and then converted to reflectance data using fast line-of-sight atmospheric analysis of spectral hypercubes (FLAASH) software.

The LiDAR data were obtained from LMS-Q560 (Riegler), which observes the first and last return pulses with a ground sampling distance of 0.5 m. The CHM used was the difference between the digital elevation model (DEM) and the DSM, and was obtained with a sampling distance of 1 m. The CHM represents the heights of trees excluding terrain effects.

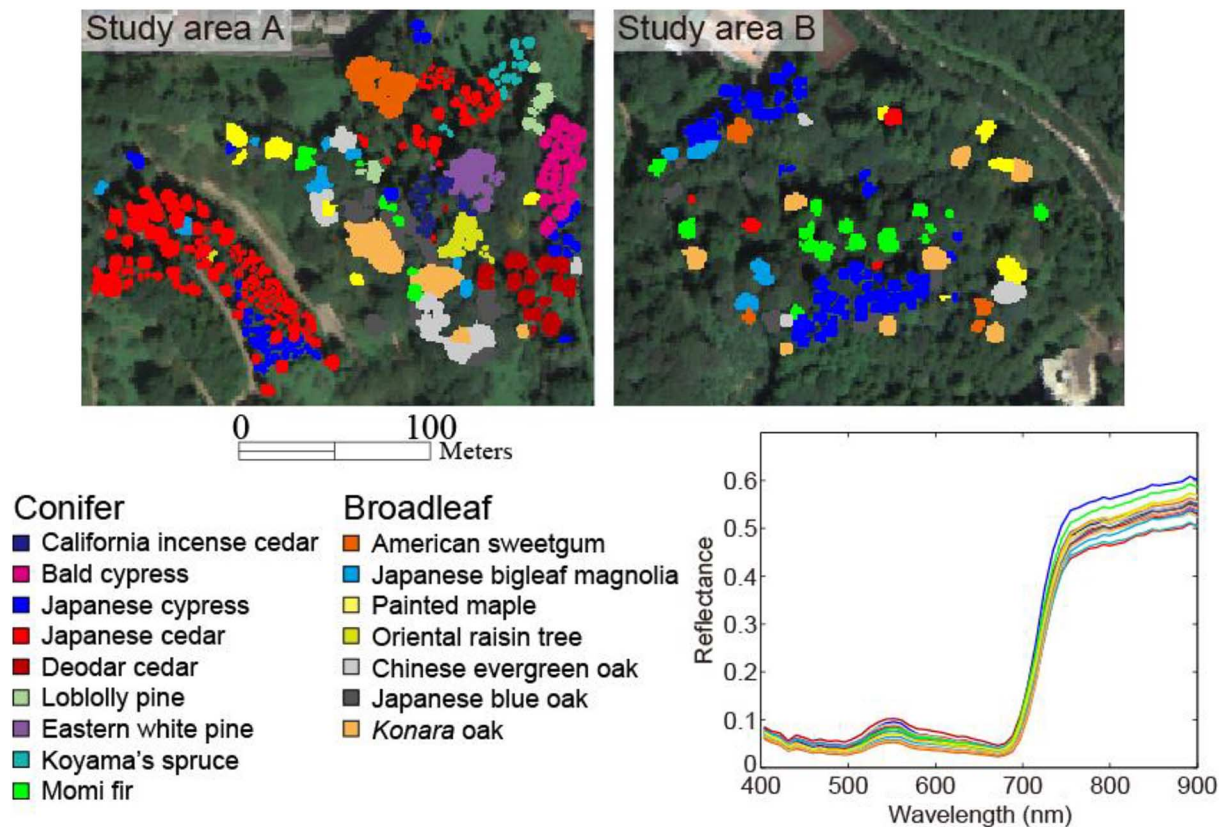


Fig. 2. Ground reference of 16 major species in the study areas and their average spectra obtained from de-shadowed hyperspectral data.

C. Field Survey Data

A field survey was carried out in this area tree by tree, by human inspection. Fig. 2 shows the distribution of the ground reference of 16 major species in the study areas and their average spectra obtained from de-shadowed hyperspectral data. The species and the crown shapes of some trees were investigated by experts. The field survey data were composed of the tree species and a shapefile showing a polygon of the tree crown for individual trees. The polygon of the tree crown was overlaid on the remote sensing data to represent the ground reference. Although there are more than 150 species of trees in this area, most of them occupy only a few pixels. We chose 16 major species with sufficient ground reference data for our investigation. Table I shows the class names and the numbers of trees and pixels. The study areas comprise typical mixed forest consisting of conifers and broadleaf trees.

III. METHODOLOGY

The proposed method consists of four parts: 1) shadow correction of the hyperspectral data; 2) individual tree-crown delineation from the LiDAR-derived CHM; 3) classification by an SVM; and 4) postprocessing. Fig. 3 shows the classification flow for the proposed methodology.

A. Shadow Correction

Shadows are a common source of intensity variability, which leads to misclassification. A great deal of attention has been

paid to removing shadows from passive optical remote sensing images. Since the structures of trees are complex owing to their complicated multilayers, the shadow correction of a forest is a challenging task. Generally, the shadow correction process comprises two steps: 1) detection and 2) de-shadowing. One common approach is the joint use of matched-filter-based thresholding for detection and an atmospheric radiative transfer model for de-shadowing [21], [22]. Several parameters for thresholding and atmospheric conditions must be carefully defined in this approach. When a DSM is available, ray tracing is effective for detecting shadows [14], [23], [24]; however, it is necessary to identify the area containing exactly the same objects as those in the shadow area for de-shadowing, which may be challenging in the case of a forest. We adopt an unmixing-based approach for shadow correction [25], since it can be fully automated and can effectively improve the classification accuracy without requiring the blue-skewed skylight illumination of the shadow.

First, the shadow is assumed to be a “black” (zero reflectance) endmember. Next, endmember spectra obtained by vertex component analysis (VCA) [26] are assumed to be unshadowed. VCA is a data-driven approach with a given number of endmembers, and the number of endmembers in this study is determined to be 15 by using HySime [27]. Abundance fractions are estimated using the fully constrained least-squares (FCLS) method satisfying sum-to-one and nonnegativity constraints [28]. The reflectance spectra are approximately de-shadowed by dividing the spectra by one minus the shadow abundance.

TABLE I
CLASS NAMES OF MAJOR TREE SPECIES WITH THE NUMBERS OF TREES AND PIXELS OF REFERENCE DATA

	English name	Scientific name	Trees	Pixels
1	California incense cedar	<i>Calocedrus decurrens</i>	20	304
2	Bald cypress	<i>Taxodium distichum</i>	33	927
3	Japanese cypress	<i>Chamaecyparis obtusa</i>	94	2995
4	Japanese cedar	<i>Cryptomeria japonica</i>	173	3492
5	Deodar cedar	<i>Cedrus deodara</i>	16	833
6	Loblolly pine	<i>Pinus taeda</i>	12	332
7	Eastern white pine	<i>Pinus strobus</i>	13	579
8	Koyama's spruce	<i>Picea koyamae</i>	14	267
9	Momi fir	<i>Abies firma</i>	22	1095
10	American sweetgum	<i>Liquidambar styraciflua</i>	11	1019
11	Japanese bigleaf magnolia	<i>Magnolia obovata</i>	12	762
12	Painted maple	<i>Acer pictum</i>	11	755
13	Oriental raisin tree	<i>Hovenia dulcis</i>	10	361
14	Chinese evergreen oak	<i>Quercus myrsinifolia</i>	14	1204
15	Japanese blue oak	<i>Quercus glauca</i>	26	1505
16	<i>Konara</i> oak	<i>Quercus serrata</i>	12	1755

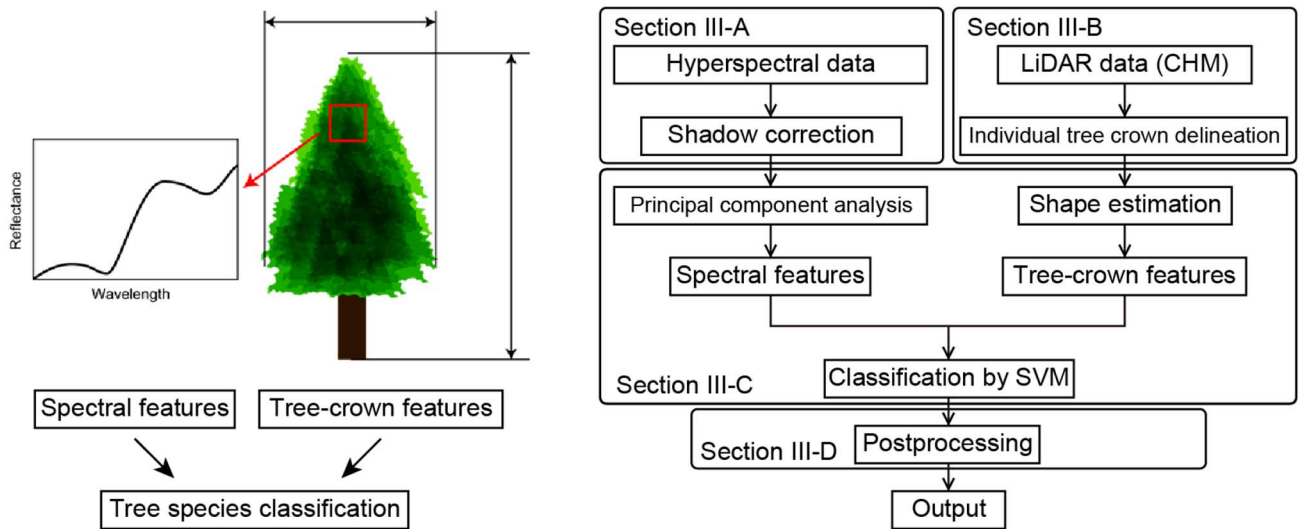


Fig. 3. Concept of data fusion and data processing flow.

B. Individual Tree-Crown Delineation

Individual tree-crown delineation is an important technique for extracting information from forests. Many researchers have investigated the use of individual tree-crown delineation methods for passive remote sensing applications, such as region growing methods, valley following methods, and so forth [29]–[36]. In this study, we use a region growing method to obtain the LiDAR-derived CHM [37], [38]. First, to reduce noise, we apply a Gaussian smoothing filter with a kernel size of three pixels to the CHM, which is selected so as not to miss small

trees. Then, we find local maxima in the smoothed image, which include nontree objects. To remove these objects, the local maxima whose normalized difference vegetation indices (NDVIs) are lower than 0.5 or whose heights are less than 1 m are excluded [14], [19]. The remaining objects correspond to the tops of trees. Regions corresponding to tree crowns are grown from the local maxima. If neighboring pixels satisfy certain conditions, a region is formed from these pixels and the neighboring pixels become the next starting pixels. The conditions are set that the height of each neighboring pixel is less

than that of the starting pixel and greater than 1 m, so that regions do not reach the ground. This growth step is repeated until there are no more starting pixels. After the growth step, each region is adjusted so that it is star-shaped to exclude the pixels that are located outside the region centered at the tree-top [37], [38]. Finally, overlapping regions are assigned to the region containing the nearest local maximum in the projected two-dimensional coordinates.

C. SVM Classification

We adopt the SVM classifier with the radial basis function (RBF) kernel to classify the pixel level using spectral and tree-crown information as input features. SVMs are widely acknowledged to be effective algorithms for pixel-level classification using hyperspectral data [39], including tree species classification [15]–[17]. The number of spectral bands of the hyperspectral data is 72, but the latent dimension is generally lower. Therefore, the principal components of the de-shadowed hyperspectral data are used as the spectral features; we input 15 principal components that represent more than 99.5% of the variance contained in the data. Then, the crown height, size, and curvature are used as tree-crown features. The height and size are defined by the highest value in the CHM and the number of pixels in each crown, respectively. The curvature is estimated by the fitting function

$$z = H - ar^c, \quad (1)$$

where we assume axial symmetry and use cylindrical coordinates (r, z) . H denotes the height of the tree, and a and c are estimated values. The Levenberg–Marquardt algorithm is used to solve the nonlinear least-squares curve-fitting problem. If a pixel is not included in any of the crowns, the height is the pixel's own value, the size is 1, and the curvature is 0. The optimal parameter of the RBF kernel is defined by cross-validation [40]. We coded this method using MATLAB with LIBSVM, which is a library of SVMs that supports multiclass classification, using the one-against-one method [41].

D. Postprocessing

Although we use tree-crown information derived from the mapping of LiDAR data as the input feature, the result of pixel-level classification includes salt-and-pepper noise owing to the spectral variability in each crown. Postprocessing in the spatial domain is effective for improving the classification outcome [42]. A majority voting procedure for the pixels in each tree crown is a common postprocessing technique when a rasterized CHM is available [17]; however, the modification entirely depends on the accuracy of individual tree-crown delineation. The use of a smoothing filter is a popular postprocessing technique to obtain better classification results. Here, we propose a crown-preserving smoothing filter inspired by bilateral filters [43], [44].

The class label at each pixel in an image is replaced by a weighted vote of the class from neighboring pixels with the aim of reducing the salt-and-pepper noise due to misclassification while preserving the crown edges. This weight can

be based on a Gaussian distribution defined by the Euclidean distance between pixels and crown segments instead of radiometric differences. If a filtered pixel belongs to the same crown as neighboring pixels, the weights of all these pixels are one; otherwise, they are smaller than one. Since the classification results are categorical values $(1, \dots, K)$, we reclassify the pixel into the class in which the weighted voting score is highest. This procedure is formulated as

$$\begin{aligned} \hat{f}(i, j) &= \operatorname{argmax}_{k \in K} \sum_{n=-w}^w \sum_{m=-w}^w \exp\left(-\frac{m^2 + n^2}{2\sigma^2}\right) I(k) P(m, n) \\ I(k) &= \begin{cases} 1, & \text{if } f(i+m, j+n) = k \\ 0, & \text{otherwise} \end{cases} \\ P(m, n) &= \begin{cases} 1, & \text{if } p(i, j) = p(i+m, j+n) > 0 \\ \alpha(0 \leq \alpha \leq 1), & \text{otherwise} \end{cases} \end{aligned} \quad (2)$$

where f is the class label obtained by the pixel-level classification and p is the index of the crown. If a pixel does not belong to any crown, then $p = 0$. The parameter α controls the consideration of crown segments, i.e., $\alpha \rightarrow 0$ means that the weight is calculated considering only the pixels in a crown, whereas $\alpha \rightarrow 1$ implies no consideration of the crowns. Therefore, the proposed filter with the parameters $w \rightarrow \infty$, $\sigma \rightarrow \infty$, and $\alpha \rightarrow 0$ is equivalent to majority voting. α is set to 0.5 to assign moderate importance to consider crown segments. σ is defined by setting the full width at half maximum of the Gaussian distribution which is equal to w . The window of the proposed filter is set to the average size of tree crowns obtained by individual tree-crown delineation, which is 11×11 pixels in this study.

IV. RESULTS AND DISCUSSION

A. Shadow Correction and Crown Delineation

Fig. 4(a) and (b) shows the de-shadowed image and the shadow map in study area A obtained by unmixing-based shadow correction, respectively. The southeast side of the trees, which is illuminated by sunshine, is bright, whereas the north-west side is darker, indicating that the amount of shadow is larger. Note that the changes in illumination resulting from the use of the DSM are also corrected. The RGB image in Fig. 4(a) shows that the shadow effect is corrected for most shadows, which appear as flat patterns in individual tree crowns owing to shadow correction, showing that a better reflectance image is obtained than that in Fig. 1. However, the correction of shadows on roads and houses is not satisfactory, although they are outside the target area in this study. The present shadow correction method does not take account of spectral dependence, which does not represent the actual situation and leads to the spectral distortion of roads and houses. Furthermore, because most of the pixels are located in the forest area, the regions of roads and houses are not selected as endmembers in the unmixing process. Further improvement in shadow correction by using ray tracing will lead to better restoration of the spectral profile of reflectance.

After applying a smoothing filter to the original CHM, the local maxima of the CHM are found and then individual tree

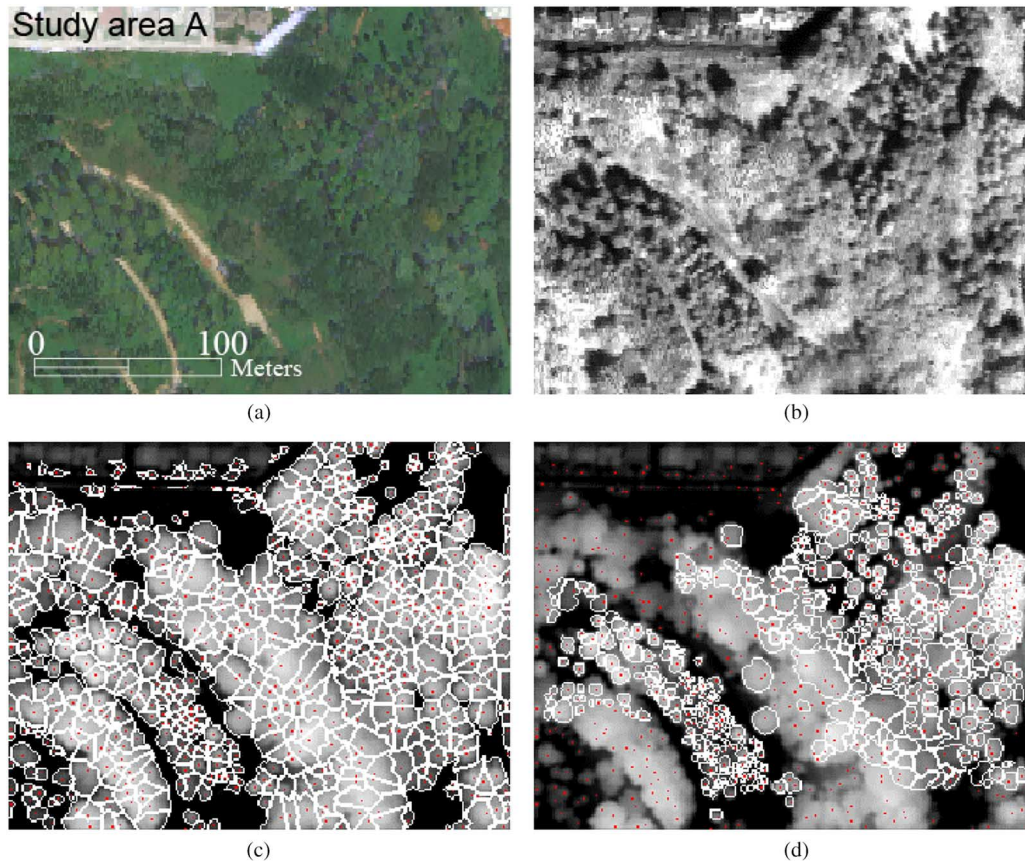


Fig. 4. (a) RGB image of de-shadowed hyperspectral data; (b) shadow map; and (c) results of individual tree-crown delineation overlaid on CHM with (d) ground reference in study area A.

crowns are selected using the thresholds of $\text{CHM} > 1 \text{ m}$ and $\text{NDVI} > 0.5$. Fig. 4(c) and (d) shows the result of individual tree-crown delineation and its ground reference in study area A, both overlaid on the CHM, respectively. The red dots represent the tops of trees that correspond to local maxima. It is found that the local maxima corresponding to houses in the upper region of the figures are excluded by this procedure. By comparison with the ground reference data, several problems in the extraction of individual tree crowns are found. Small trees with a high density located in the southwest area are not extracted. Moreover, large trees have several local maxima in the tree crown, which originate from the region growing method, resulting in a single tree being separated into several small tree crowns. These problems are related to the smoothing process and further improvements are needed in adaptive data processing. Furthermore, small trees under a tall tree are not distinguished because their local maxima are not found. Although waveform LiDAR can solve this problem [9], it is difficult to distinguish a layered structure using the proposed method.

B. Tree-Crown Classification

We applied the SVM classifier to the input features obtained by the proposed method and compared the classification results with those obtained with and without shadow correction and the use of tree-crown information. Since the number of trees is limited for each tree species in the ground reference, e.g., less

than 15 for 9 of the species, it is very challenging to obtain tree-crown features via tree-wise sampling using reference polygons. In this work, we first adopted the random sampling of pixels to select training samples, assuming that almost all the tree-crown variations are included in the training set. The training set size is given as a percentage of the entire ground reference and the remaining reference pixels were used for validation in each trial. Fig. 5 shows the classification maps and the overall accuracy (OA) of one trial when the training set size is 10%. The accuracy of the classification map obtained by the proposed method is greater than those of the maps obtained using spectral features only, de-shadowed spectral features only, and spectral and tree-crown features. In study area A, owing to shadow correction, we can see an improvement in the classification results in the central area and in the area of Koyama's spruce in the northeast. Furthermore, the salt-and-pepper noise is mitigated by the proposed method by using the tree-crown features. Table II shows the confusion matrix of the proposed method along with the producer's accuracy (PA) and user's accuracy (UA) for all classes. The PAs for Japanese cypress and cedars are reasonably high owing to the use of a large number of training samples covering a wide range of within-class variability; however, this leads to the misclassification of pixels belonging to other classes, which is indicated by their relatively low PAs.

Fig. 6 shows the PA of each class for the four methods, which is obtained by averaging the results of 10 trials. The proposed

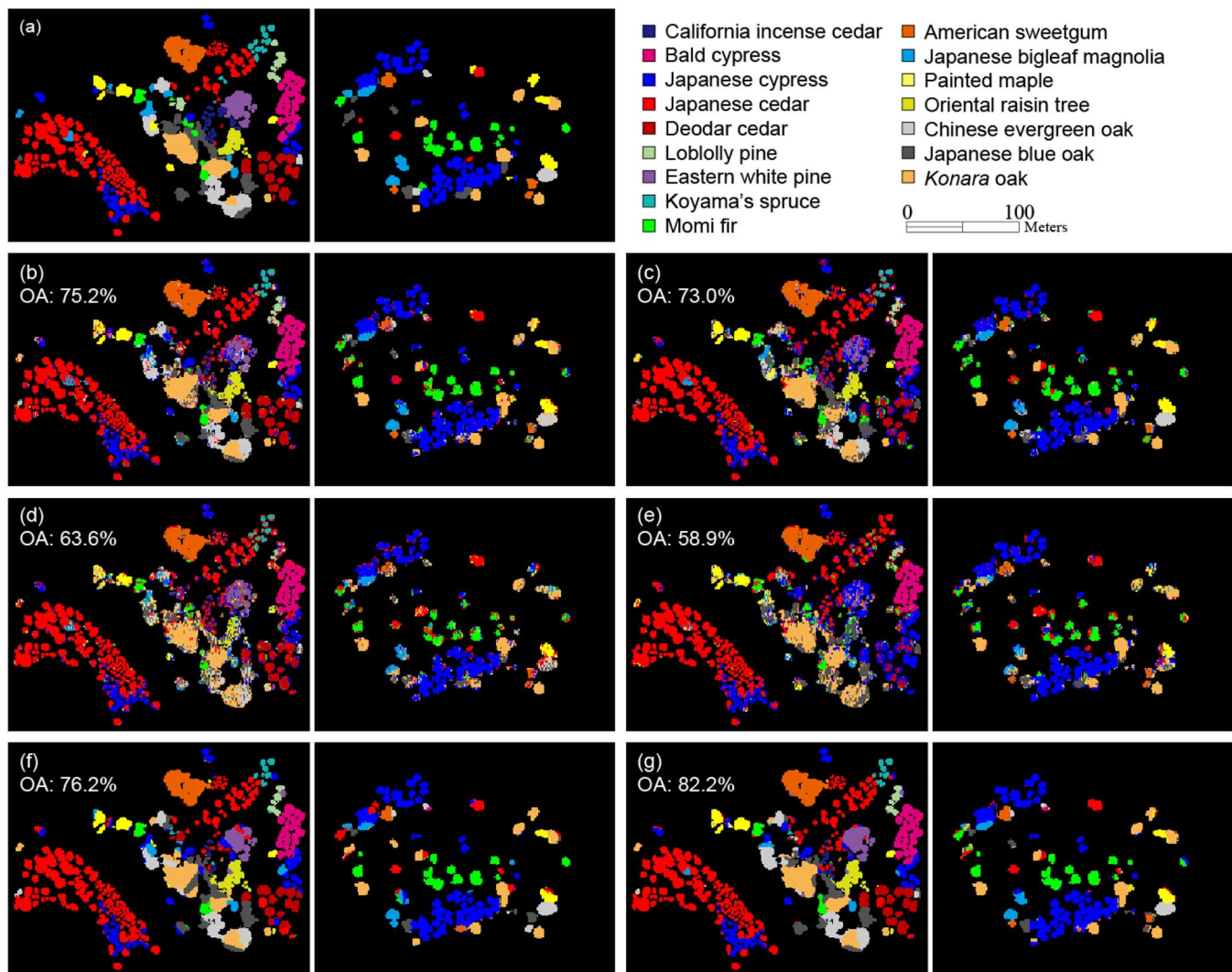


Fig. 5. Classification map of (a) ground reference and classification maps obtained using; (b) de-shadowed spectral and tree-crown features; (c) spectral and tree-crown features, (d) de-shadowed spectral features only; and (e) spectral features only. Classification maps after (f) majority voting and (g) applying the proposed filter to the map in (b).

method is more accurate than the other methods for many of the classes. In particular, the joint use of the tree-crown features derived from the CHM improves the results for California incense cedars, Loblolly pines, Koyama's spruces, and Oriental raisin trees, whereas those obtained using only spectral features show lower accuracies. The overall accuracy is shown in Fig. 7(a) for the six methods with training set sizes of 1% to 30% to examine the effects of the use of shadow correction, tree-crown features, and feature extraction from the CHM in addition to shadow correction. For each size of the training set, the average accuracy of 10 trials is plotted. When the training set size is larger than 10%, shadow correction and the use of tree-crown features increase the accuracy by 2.5% and 12%, respectively. These results indicate that shadow correction based on unmixing has a positive impact on tree species classification, and that the tree-crown features are effective for improving the pixel-level classification, which is difficult to discriminate using only spectral features.

Fig. 7(a) also shows a comparison of the classification results obtained by individual tree-crown delineation of the ground

reference collected by experts, the region growing image processing used in this study and the original CHM as well as the results obtained without the use of the CHM to demonstrate the impact of feature extraction using the CHM in addition to the de-shadowed spectral features. The proposed method clearly outperforms the method using the original pixel values of the CHM. The use of the ground reference obtained by individual tree-crown delineation increases the accuracy by 4% compared with that of the proposed method, which implies that better individual tree-crown delineation may improve classification results.

C. Postprocessing

Fig. 5(f) and (g), respectively, shows the postprocessed maps obtained by majority voting and using the proposed filter with 10% of the ground reference as training samples. The proposed filter can smooth results while preserving smaller structures more effectively than majority voting. Fig. 7(b) shows the overall accuracy of the classification results obtained with

TABLE II
CONFUSION MATRIX

Class	1	2	3	4	5	6	7	8	9	10	11	12	13	14	15	16	Total	PA	
1	112	0	57	71	2	0	3	2	1	0	0	0	22	0	2	1	273	0.41	
2	1	728	52	12	5	0	9	0	0	1	19	0	0	0	2	0	829	0.88	
3	3	0	2383	136	30	0	2	1	11	12	10	5	22	17	18	29	2679	0.89	
4	10	33	156	2815	2	2	3	5	23	17	29	2	16	9	26	4	3152	0.89	
5	1	0	41	74	586	6	7	3	10	4	1	0	7	0	4	3	747	0.78	
6	0	0	15	35	67	140	27	4	2	1	4	0	0	0	0	1	296	0.47	
7	7	0	82	49	26	0	319	3	0	0	5	0	1	27	1	11	531	0.60	
8	0	10	11	85	0	0	4	123	0	0	0	0	3	0	1	0	237	0.52	
9	0	1	72	62	4	0	0	9	728	1	5	2	0	13	25	48	970	0.75	
10	0	7	22	13	2	0	11	0	8	741	5	0	0	46	48	8	911	0.81	
11	0	2	126	41	0	0	3	2	9	4	349	8	14	8	39	84	689	0.51	
12	0	1	44	57	0	0	0	0	1	15	6	429	0	53	11	68	685	0.63	
13	0	0	12	11	0	0	18	0	0	1	0	0	267	6	8	0	323	0.83	
14	0	15	67	21	1	0	2	0	6	10	20	5	0	666	137	154	1106	0.60	
15	2	9	107	56	2	0	2	0	30	24	7	6	29	135	704	257	1370	0.51	
16	0	0	40	39	4	0	31	0	7	6	22	13	6	29	156	1215	1568	0.77	
Total	136	806	3287	3577	731	148	441	152	836	837	482	470	387	1011	1182	1883	16366		
UA	0.82	0.90	0.73	0.79	0.80	0.95	0.72	0.81	0.87	0.89	0.72	0.91	0.69	0.66	0.60	0.65			
																		OA	0.75

postprocessing. The proposed filter improves the overall accuracy by 7%, whereas majority voting increases the accuracy by 1%. Therefore, the proposed methodology increases the accuracy by a total of 21.5% when using 10% training data. Although the results obtained by postprocessing depend on the delineation, the proposed filter can preserve small structures even if the delineation is incomplete. For example, in the west part of study area A in Fig. 5(f), the majority voting misclassified a small area of Japanese bigleaf magnolias surrounded by Japanese cedars into the latter because the size of individual tree crowns of the latter species was overestimated. In contrast, the proposed method correctly modified class labels of pixels in this area because the number of pixels classified as Japanese bigleaf magnolias in each delineated crown is comparable to the number classified as Japanese cedars. The result shows that the proposed crown-preserving smoothing filter has the potential to moderately improve classification results by considering delineated crowns even though they include errors.

D. Accuracy Assessment Using Reference Polygons

When the validation samples are allowed to be in the same polygons (i.e., trees in this study) as the training samples, the classification accuracy can be overestimated owing to the

strong correlation between the training and validation data [45]. To perform a more practical assessment, we conducted experiments involving tree-wise sampling by separating the ground reference data tree by tree with a ratio of four to one between the training and validation data. The training set was randomly sampled on a pixel basis and its size is given as a percentage of the separated training data. Fig. 8 shows the overall accuracy obtained with this validation scenario. In Fig. 8(a), the relationship between the six methods is similar to that shown in Fig. 7(a) and the proposed method gives the best result with a 3%–4% increase in the accuracy compared with that obtained using spectral features only. However, the overall accuracy for all the methods is lower than that in Fig. 7(a) obtained using pixel-based random sampling for accuracy assessment. This implies that sufficient training data are required to include the within-class variation of tree-crown features for each class to improve the classification performance of the proposed method. As shown in Fig. 8(b), the proposed filter increases the accuracy by 5%, whereas majority voting reduces the accuracy. Our approach increases the accuracy by a total of approximately 9%, which proves the efficacy of the proposed methodology for practical assessment. This work shows that hyperspectral data with tree-crown features are effective for tree species classification in Japanese forests, in which conifers and broadleaf trees result in complex biodiversity.

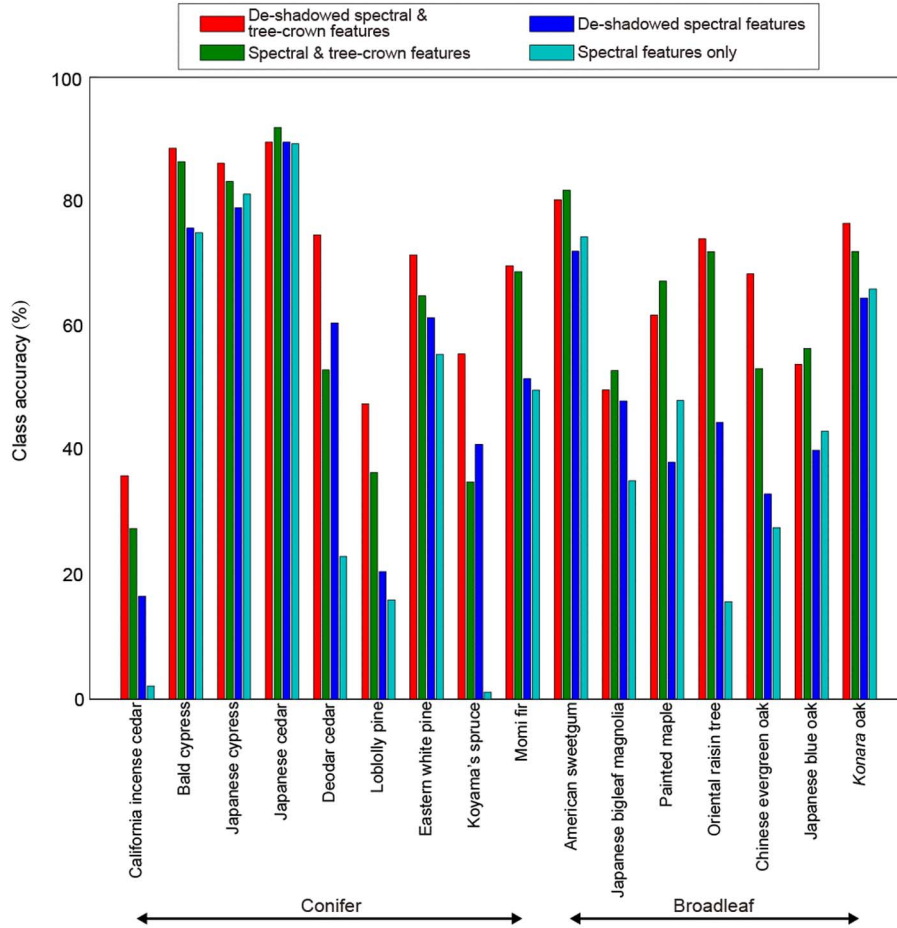


Fig. 6. PA of 16 major tree species.

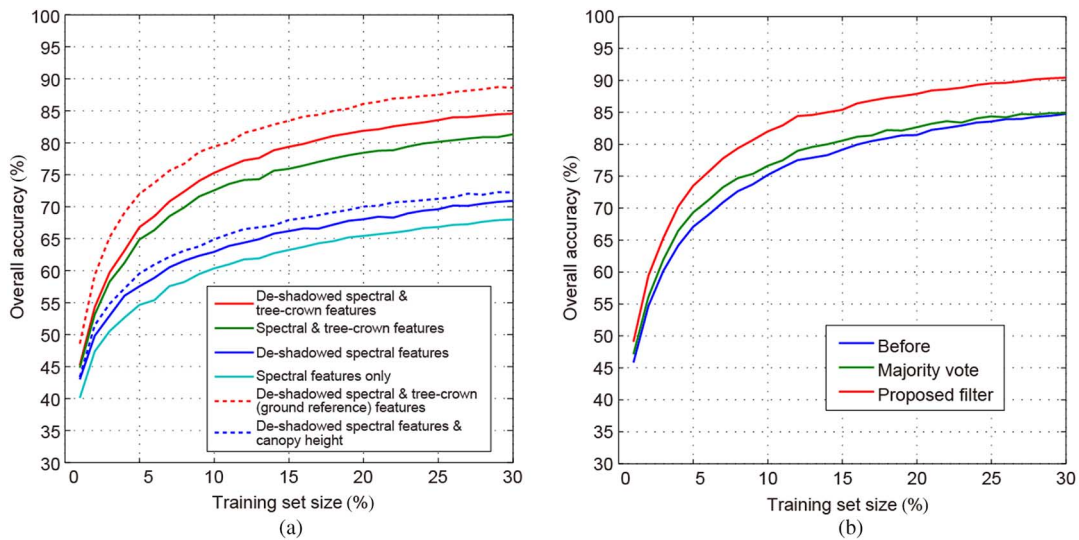


Fig. 7. Overall accuracy of tree species classification. (a) Comparison of six methods to examine effects of the use of shadow correction, tree-crown features, and feature extraction from CHM in addition to shadow correction. (b) Effects of postprocessing.

V. CONCLUSION

We presented a methodology to classify tree species using hyperspectral data and a LiDAR-derived CHM. Shadow correction is applied to hyperspectral data, and information on

the tree size and shape is obtained after individual tree delineation of the CHM. The SVM classifier is used for pixel-level classification, which is followed by postprocessing using a crown-preserving smoothing filter. The proposed method was

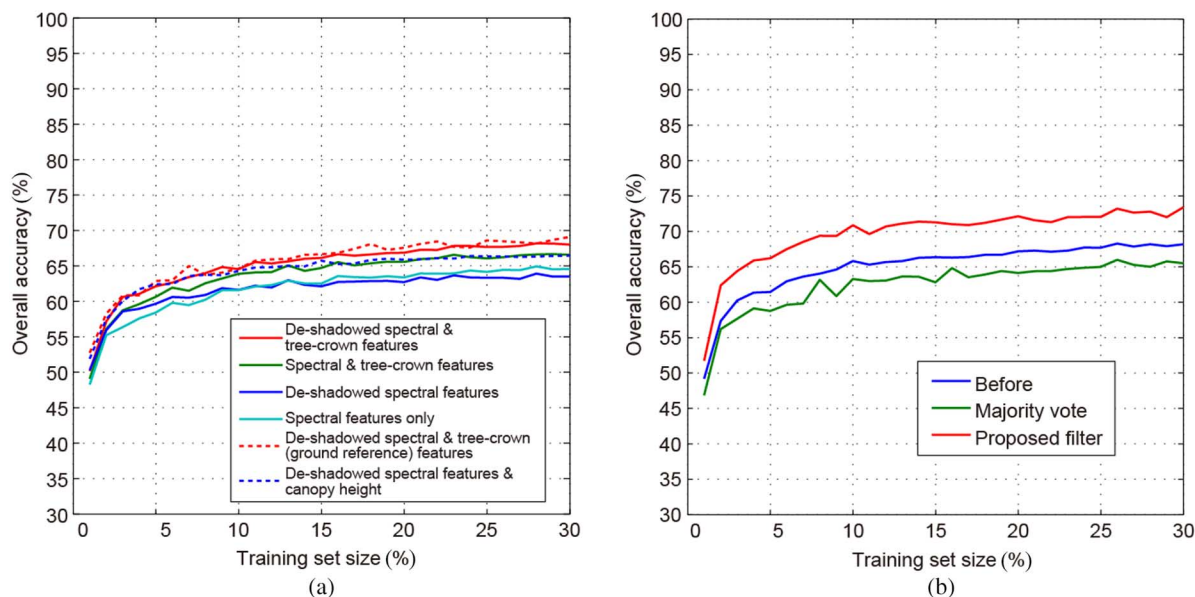


Fig. 8. Overall accuracy of tree species classification using reference polygons. (a) Comparison of six methods to examine effects of the use of shadow correction, tree-crown features, and feature extraction from CHM in addition to shadow correction. (b) Effects of postprocessing.

applied to a dataset taken over Tama Forest Science Garden in Tokyo, Japan, to classify the data into 16 classes. Both shadow correction and the use of tree-crown features derived from the CHM markedly improved the classification accuracy. In particular, individual tree-crown delineation, which is also used in the postprocessing, made a major contribution to the accurate classification of tree species in the complex mixed forest, showing the importance of LiDAR data. Our results indicate that the fusion of remote sensing data will be useful for forest management in Japan, one-third of which is covered with forests. This methodology can be extended to very high-resolution imagery by incorporating it in a DSM derived from stereovision, which provides detailed tree-crown information. Our future work includes transfer learning for tree species classification considering more practical conditions.

REFERENCES

- [1] S. E. Franklin, *Remote Sensing for Sustainable Forest Management*. Boca Raton, FL, USA: CRC Press, 2001.
- [2] D. Goodenough *et al.*, "Processing hyperion and ALI for forest classification," *IEEE Trans. Geosci. Remote Sens.*, vol. 41, no. 6, pp. 1321–1331, Jun. 2003.
- [3] D. G. Leckie *et al.*, "Issues in species classification of trees in old growth conifer stands," *Can. J. Remote Sens.*, vol. 31, no. 2, pp. 175–190, 2005.
- [4] M. L. Clark, D. A. Roberts, and D. B. Clark, "Hyperspectral discrimination of tropical rain forest tree species at leaf to crown scales," *Remote Sens. Environ.*, vol. 96, no. 3–4, pp. 375–398, 2005.
- [5] M. Martin, S. Newman, J. Aber, and R. Congalton, "Determining forest species composition using high spectral resolution remote sensing data," *Remote Sens. Environ.*, vol. 65, no. 3, pp. 249–254, 1998.
- [6] M. Dalponte, L. Bruzzone, L. Vescovo, and D. Gianelle, "The role of spectral resolution and classifier complexity in the analysis of hyperspectral images of forest areas," *Remote Sens. Environ.*, vol. 113, no. 11, pp. 2345–2355, 2009.
- [7] M. Fauvel, J. A. Benediktsson, J. Chanussot, and J. R. Sveinsson, "Spectral and spatial classification of hyperspectral data using SVMs and morphological profiles," *IEEE Trans. Geosci. Remote Sens.*, vol. 46, no. 11, pp. 3804–3814, Nov. 2008.
- [8] E. Næsset, "Estimating timber volume of forest stands using airborne laser scanner data," *Remote Sens. Environ.*, vol. 61, no. 2, pp. 246–253, 1997.
- [9] J. Hyypä, O. Kelle, M. Lehtikainen, and M. Inkinen, "A segmentation-based method to retrieve stem volume estimates from 3-D tree height models produced by laser scanners," *IEEE Trans. Geosci. Remote Sens.*, vol. 39, no. 5, pp. 969–975, May 2001.
- [10] J. Holmgren and Å. Persson, "Identifying species of individual trees using airborne laser scanner," *Remote Sens. Environ.*, vol. 90, pp. 415–423, 2004.
- [11] W. Yao, P. Krzystek, and M. Heurich, "Tree species classification and estimation of stem volume and DBH based on single tree extraction by exploiting airborne full-waveform LiDAR data," *Remote Sens. Environ.*, vol. 123, pp. 368–380, 2012.
- [12] G. A. Blackburn, "Remote sensing of forest pigments using airborne imaging spectrometer and LiDAR imagery," *Remote Sens. Environ.*, vol. 82, no. 2–3, pp. 311–321, 2002.
- [13] R. Sugumaran and M. Voss, "Object-oriented classification of lidar-fused hyperspectral imagery for tree species identification in an urban environment," in *Proc. Urban Remote Sens. Joint Event*, 2007, pp. 1–6.
- [14] G. P. Asner *et al.*, "Invasive species detection in Hawaiian rainforests using airborne imaging spectroscopy and LiDAR," *Remote Sens. Environ.*, vol. 112, pp. 1942–1955, 2008.
- [15] M. Dalponte, L. Bruzzone, and D. Gianelle, "Fusion of hyperspectral and lidar remote sensing data for classification of complex forest areas," *IEEE Trans. Geosci. Remote Sens.*, vol. 46, no. 5, pp. 1416–1427, May 2008.
- [16] M. Dalponte, L. Bruzzone, and D. Gianelle, "Tree species classification in the Southern Alps based on the fusion of very high geometrical resolution multispectral/hyperspectral images and LiDAR data," *Remote Sens. Environ.*, vol. 123, pp. 258–270, 2012.
- [17] M. Dalponte, H. O. Ørka, L. T. Ene, T. Gobakken, and E. Naeset, "Tree crown delineation and tree species classification in boreal forests using hyperspectral and ALS data," *Remote Sens. Environ.*, vol. 140, pp. 306–317, Jan. 2014.
- [18] T. G. Jones, N. C. Coops, and T. Sharma, "Assessing the utility of airborne hyperspectral and LiDAR data for species distribution mapping in the coastal Pacific Northwest, Canada," *Remote Sens. Environ.*, vol. 114, pp. 2841–2852, 2010.
- [19] M. Alonzo, B. Bookhagen, and D. A. Roberts, "Urban tree species mapping using hyperspectral and LiDAR data fusion," *Remote Sens. Environ.*, vol. 148, pp. 70–83, 2014.
- [20] Forestry and Forest Products Research Institute, *Tama Forest Science Garden* [Online]. Available: <http://www.ffpri.affrc.go.jp/tmk/en/index.html>, accessed on Feb. 2, 2015.
- [21] S. M. Adler-Golden, M. W. Matthew, G. P. Anderson, G. W. Felde, and J. A. Gardner, "An algorithm for de-shadowing spectral imagery," in *Proc. 11th JPL Airborne Earth Sci. Workshop*, 2002, pp. 1–8.
- [22] R. Richter and A. Müller, "De-shadowing of satellite/airborne imagery," *Int. J. Remote Sens.*, vol. 26, no. 15, pp. 3137–3148, 2005.

- [23] O. Friman, G. Tolt, and J. Ahlberg, "Illumination and shadow compensation of hyperspectral images using a digital surface model and non-linear least squares estimation," in *Proc. SPIE 8180 Image Signal Process. Remote Sens. XVII*, vol. 8180Q, 2011, pp. 1–8.
- [24] Y. Li, P. Gong, and T. Sasagawa, "Integrated shadow removal based on photogrammetry and image analysis," *Int. J. Remote Sens.*, vol. 26, no. 18, pp. 3911–3929, 2005.
- [25] J. W. Boardman, "Automating spectral unmixing of AVIRIS data using convex geometry concepts," in *Proc. Summaries 4th Annu. JPL Airborne Geosci. Workshop*, 1993, vol. 1, pp. 11–14. JPL Publication 93–26.
- [26] J. M. P. Nascimento and J. M. B. Dias, "Vertex component analysis: A fast algorithm to unmix hyperspectral data," *IEEE Trans. Geosci. Remote Sens.*, vol. 43, no. 4, pp. 898–910, Apr. 2005.
- [27] J. Bioucas-Dias and J. Nascimento, "Hyperspectral subspace identification," *IEEE Trans. Geosci. Remote Sens.*, vol. 46, no. 8, pp. 2435–2445, Aug. 2008.
- [28] D. Heinz and C.-I. Chang, "Fully constrained least squares linear spectral mixture analysis method for material quantification in hyperspectral imagery," *IEEE Trans. Geosci. Remote Sens.*, vol. 39, no. 3, pp. 529–545, Mar. 2001.
- [29] Y. Ke and L. J. Quackenbush, "A review of methods for automatic individual tree crown detection and delineation from passive remote sensing," *Int. J. Remote Sens.*, vol. 32, no. 17, pp. 4725–4747, 2011.
- [30] M. Erikson and K. Olofsson, "Comparison of three individual tree crown detection methods," *Mach. Vision Appl.*, vol. 16, no. 4, pp. 258–265, 2005.
- [31] R. J. Pollock, "The automatic recognition of individual trees in aerial images of forests based on a synthetic tree crown image model," Ph.D. dissertation, Dept. Comput. Sci., Univ. British Columbia, 1996.
- [32] K. Olofsson, J. Wallerman, J. Holmgren, and H. Olsson, "Tree species discrimination using Z/I DMC imagery and template matching of single trees," *Scand. J. For. Res.*, vol. 21, no. S7, pp. 106–110, 2006.
- [33] M. Erikson, "Segmentation of individual tree crowns in color aerial photographs using region growing supported by fuzzy rules," *Can. J. For. Res.*, vol. 33, no. 8, pp. 1557–1563, 2003.
- [34] M. Erikson, "Species classification of individually segmented tree crowns in high resolution aerial images using radiometric and morphologic image measures," *Remote Sens. Environ.*, vol. 91, no. 3–4, pp. 469–477, 2004.
- [35] F. A. Gougeon, "A crown-following approach to the automatic delineation of individual tree crowns in high spatial resolution aerial images," *Can. J. Remote Sens.*, vol. 21, no. 3, pp. 274–284, 1995.
- [36] Z. Li, R. Hayward, J. Zhang, and Y. Liu, "Individual tree crown delineation techniques for vegetation management in power line corridor," in *Proc. Digital Image Comput. Techn. Appl. (DICTA)*, 2008, pp. 148–154.
- [37] B. Koch, U. Heyder, and H. Weinacker, "Detection of individual tree crowns in airborne lidar data," *Photogramm. Eng. Remote Sens.*, vol. 72, no. 4, pp. 357–363, 2006.
- [38] S. Solberg, E. Naesset, and O. M. Bollandsas, "Single tree segmentation using airborne laser scanner data in a structurally heterogeneous spruce forest," *Photogramm. Eng. Remote Sens.*, vol. 72, no. 12, pp. 1369–1378, 2006.
- [39] F. Melgani and L. Bruzzone, "Classification of hyperspectral remote sensing images with support vector machines," *IEEE Trans. Geosci. Remote Sens.*, vol. 42, no. 8, pp. 1778–1790, Aug. 2004.
- [40] C. M. Bishop, *Pattern Recognition and Machine Learning (Information Science and Statistics)*. New York, NY, USA: Springer-Verlag, 2006.
- [41] C. Chang and C. Lin, "LIBSVM: A library for support vector machines," *ACM Trans. Intell. Syst. Technol.*, vol. 2, no. 3, pp. 27:1–27:27, 2011 [Online]. Available: <http://www.csie.ntu.edu.tw/~cjlin/libsvm>, accessed on Aug. 18, 2013.
- [42] University of Houston, *Outcome of the "Best Classification Challenge" of the 2013 IEEE GRSS Data Fusion Contest* [Online]. Available: http://hyperspectral.ee.uh.edu/?page_id=695, accessed on Sep. 25, 2014.
- [43] C. Tomasi and R. Manduchi, "Bilateral filtering for gray and color images," in *Proc. 6th Int. Conf. Comput. Vis.*, 1998, pp. 839–846.
- [44] P. Choudhury and J. Tumblin, "The trilateral filter for high contrast images and meshes," in *Proc. ACM SIGGRAPH 2005 Courses (SIGGRAPH'05)*, New York, NY, USA, 2005, pp. 1–12.
- [45] Z. Zhen, L. J. Quackenbush, S. V. Stehman, and L. Zhang, "Impact of training and validation sample selection on classification accuracy and accuracy assessment when using reference polygons in object-based classification," *Int. J. Remote Sens.*, vol. 34, no. 19, pp. 6914–6930, 2013.



Tomohiro Matsuki received the M.Sc. degree in aerospace engineering from the University of Tokyo, Tokyo, Japan, in 2014.

His research interests include hyperspectral data analysis.



Naoto Yokoya (S'10–M'13) received the M.Sc. and Ph.D. degrees in aerospace engineering from the University of Tokyo, Tokyo, Japan, in 2010 and 2013, respectively.

From 2012 to 2013, he was a Research Fellow with the Japan Society for the Promotion of Science, Tokyo, Japan. Currently, he is an Assistant Professor with the University of Tokyo. His research interests include image processing and pattern recognition for remote sensing.



Akira Iwasaki received the M.Sc. degree in aerospace engineering and the Doctoral degree in engineering from the University of Tokyo, Tokyo, Japan, in 1987 and 1996, respectively.

In 1987, he joined the Electrotechnical Laboratory, where he was engaged in research on space technology and remote sensing system. Currently, he is a Professor with the University of Tokyo.